



TECHNICAL ARTICLE

Microstructure and Thickness Effects on Impact Behavior and Separation Formation in X70 Pipeline Steel

EMILY B. MITCHELL ^{1,4} ENRICO LUCON,² LAURIE E. COLLINS,³
AMY J. CLARKE,¹ and KESTER D. CLARKE¹

1.—Department of Material and Metallurgical Engineering, Colorado School of Mines, Golden, CO 80401, USA. 2.—Applied Chemicals and Materials Division, National Institute of Standards and Technology, Boulder, CO 80303, USA. 3.—Process and Product Development, EVRAZ North America, Regina, SKS4P3C7, Canada. 4.—e-mail: emitchel@mines.edu

In an effort to optimize the transportation of oil and gas, the pipeline industry is developing large-diameter, thick-walled pipelines that can withstand low temperatures and high pressures. In this study, three X70 steel plates of similar chemistry, ranging in thickness from 13.5 mm to 22 mm, were subjected to drop-weight tear and Charpy V-notch tests to determine the effects of plate thickness and microstructure on the formation of separations and impact behavior. Constraint induced by specimen thickness appears to dictate the location of separations, the three microstructures exhibited different separation behaviors, and microstructural banding was not found to promote separation formation. Separations were most frequent when the primary fracture plane was parallel to the rolling direction. This study also found that standardized empirical relationships between Charpy V-notch and drop-weight tear tests do not estimate to the advanced high-strength and -toughness steels investigated.

INTRODUCTION

Pipeline steels must have increasingly higher strengths and toughness to improve reliability and reduce the risk of leaks and spills,^{1,2} and demand for larger-diameter pipelines has increased interest in thicker American Petroleum Institute (API) grade plate steel.³ X70 pipeline steel microstructures vary with processing, alloying, and final plate thickness. Thermomechanical controlled processing, with the addition of accelerated cooling and inline quenching and tempering, results in many possible microstructures, including combinations of bainite, martensite, martensite–austenite (MA), ferrite–pearlite, polygonal ferrite (PF), and acicular ferrite.^{4–8} Lower toughness 45° from the rolling direction (RD) is a concern for pipeline manufacturers,^{3–5} especially when the pipeline manufacturing process is spiral

welding. Numerous studies have determined that crystallographic texture contributes to lower toughness in the 45° orientation, because this orientation typically contains a higher volume fraction of grains with cleavage planes parallel to the primary fracture plane.^{5,9,10}

Separations are splits that form parallel to the rolling plane perpendicular to the primary fracture plane of Charpy V-notch (CVN) and drop-weight tear test (DWTT) specimens because the steel has effectively delaminated during impact testing. The effects of microstructure, crystallographic texture, and banding on separation formation during CVN and DWTT testing have been investigated,^{2,5,6,9–13} but there is no consensus on the primary cause or even if separations have a negative effect on pipeline performance.^{2,14} Thicker plates are more susceptible to separations due to high through-thickness constraint, and an out-of-plane constraint factor, T_z , has been developed to describe the 3D stress state near the crack tip in compact tension specimens that exhibit separations.¹⁴ T_z is greatest at the centerline, increases with thickness, and promotes separation formation, which, coupled with

(Received March 19, 2020; accepted January 7, 2021)

microstructural features and potential defects at the plate centerline, could lead to increased separation severity. This study evaluated the effect of thickness, microstructure, and specimen orientation on impact behavior, fracture surface appearance, and separation formation in CVN and DWTT specimens.

EXPERIMENTAL METHODS

X70 plates with similar composition and three thicknesses were used for this study (Table I). Through-thickness microstructures were examined with light optical and scanning electron microscopy. Volume fraction analysis of a bainitic secondary constituent in the 22-mm plate and grain size analysis on all the plates were performed according to ASTM E562-11¹⁵ and ASTM-E112-13,¹⁶ respectively, using ImageJ. Automated Vickers microhardness (100 g, 10 s dwell) traverses were performed through-thickness every 100 μm .

Standard CVN specimens were machined with the notch normal to the plate surface in three orientations, 0°, 45°, and 90°, from RD and tested according to ASTM E23-18.¹⁷ Absorbed energy, lateral expansion (LE), and shear fracture appearance (SFA) were measured, and transition curves were generated. The transition temperature (TT) was calculated as the temperature corresponding to 50 % of the upper shelf of the transition curve (FATT₅₀).

Standard pressed notch DWTT specimens were machined in accordance with API RP-5L3¹⁸ from the plates in the same three orientations as the CVN specimens. In accordance with ASTM E436-03(2014),¹⁹ DWTT temperatures were chosen iteratively, first by establishing upper and lower shelf temperatures, and then by choosing two intermediate test temperatures to characterize the TT region. The ductile to brittle transition temperature (DBTT₈₅) was calculated as the temperature with 85% shear area (SA). Test temperatures used for CVN and DWTT can be found in Table II.

DWTT specimen fracture surfaces were photographed and shear area % (SA) measurements were performed using the line and measurement tools in ImageJ. In accordance with API RP-5L3, the lesser of the plate thicknesses or 19 mm was removed from the fracture area at the notch root and the opposite side. Equation 1 was used to determine the SA;¹⁷

$$\% SA(API) = \frac{(71 - 2t)t - 3/4(ab + a'b')}{(71 - 2t)t} \times 100 \quad (1)$$

where t is the specimen thickness, a is the cleavage fracture width one specimen thickness from the notch root, and b is the length cleavage fracture extends into the specimen from a . b was determined through visual assessment of the fracture surface and measured using ImageJ. a' and b' are the same as a and b , but for the hammer-impacted region of the specimen. The area of separations on the

Table I. Chemical composition of X70 plates in weight%

	<u>C</u>	<u>Mn</u>	<u>Si</u>	<u>Cr</u>	<u>Mo</u>	<u>Al</u>	<u>Ni</u>	<u>S</u>	<u>P</u>	<u>Cu</u>	<u>Ti + Nb + V</u>
13.5 mm	0.052	1.57	0.21	0.12	0.21	0.04	0.02	0.003	0.010	0.03	≤0.10
15.5 mm	0.050	1.51	0.20	0.14	0.16	0.03	0.01	0.002	0.005	0.01	≤0.09
22 mm	0.040	1.62	0.23	0.16	NR	0.03	NR	0.004	0.013	NR	≤0.06

NR Not reported.

Table II. CVN and DWTT test matrix

Thickness (mm) and orientation		CVN test temperatures (°C)	DWTT test temperatures (°C)
13.5	0°	-180, -135, -115, -100, -95, -90, -75, -40, -40, 21	-20, -40, -60
	45°	-180, -135, -115, -90, -70, -60, -50, -40, -40, 21	-20, -40, -50, -60
	90°	-180, -135, -115, -90, -70, -40, -10, 21, 100, 200	-20, -40, -60, -70
15.5	0°	-180, -135, -115, -100, -100, -90, -75, -40, -40, 21	-20, -25, -30, -40
	45°	-180, -135, -115, -90, -70, -65, -60, -40, -10, 21	-0, -10, -20, -30, -40
	90°	-180, -135, -115, -90, -75, -40, -40, -30, 21, 100	-20, -25, -30, -40
22	0°	-180, -135, -120, -115, -100, -95, -90, -40, -40, 21	-20, -40, -50, -60
	45°	-180, -135, -115, -110, -105, -100, -90, -40, 21, 100	-20, -40, -50, -60
	90°	-180, -135, -130, -125, -120, -115, -110, -90, -40, 21	-20, -30, -40, -60

fracture plane was included. The line-length of all the separations and the inspected fracture surface area were also measured. Separation indexes (SIs) were calculated using Eq. 2:²⁰

$$SI = \frac{\text{total length of all separations}}{\text{inspected area}} (mm^{-1}) \quad (2)$$

Inspected fracture surface areas were divided into six equal through-thickness regions to determine SIs at the edge, quarter-depth, and centerline of the specimens.

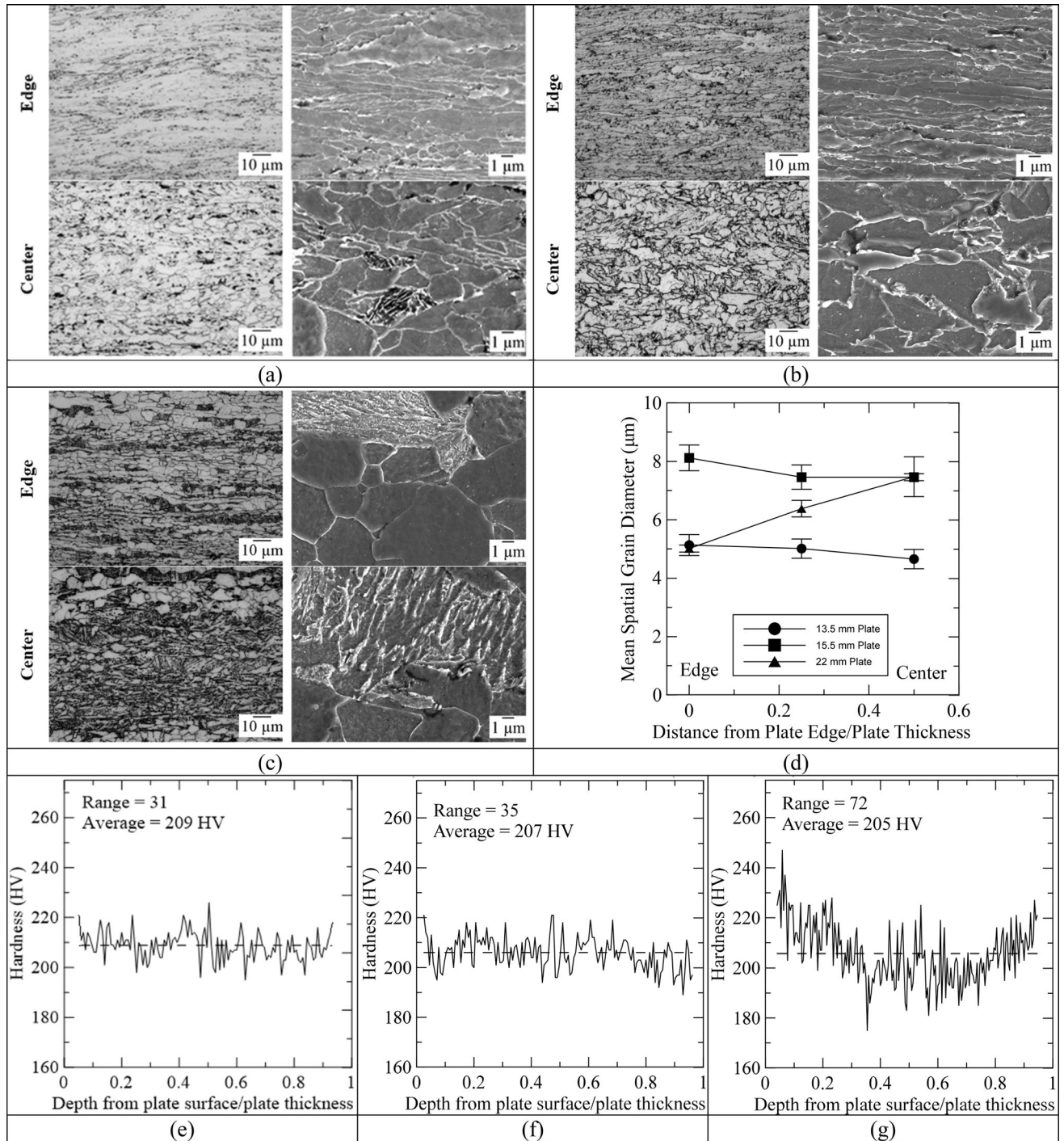


Fig. 1. Light optical and scanning electron micrographs of the (a) 13.5-mm, (b) 15.5-mm, and (c) 22-mm plates. (d) Mean grain diameter (D , μm) versus distance from plate edge normalized by plate thickness (error bars 95 % confidence interval). (e–g) Vickers microhardness (100 g, 10 s dwell time) versus depth from the plate surface measured on longitudinal sections for the (e) 13.5-mm, (f) 15.5-mm, and (g) 22-mm plates.

RESULTS

The microstructures of the 13.5-mm and 15.5-mm plates are fine equiaxed PF at the centerline with elongated grains at the edge (see Fig. 1a, b). The 13.5-mm plate contains some pearlite, with greater volume fractions toward the centerline of the plate. The microstructure of the 22-mm plate is banded and contains non-uniformly distributed ferrite and a bainitic secondary constituent, with some small, irregular regions of MA at the centerline (Fig. 1c). The volume fraction of the bainitic secondary constituent increases from ~0.25 at the edge to ~0.5 at the centerline. The two thinner plates have relatively similar grain sizes across the through-thickness, but the edge of the 22-mm plate has a finer

ferrite microstructure than the centerline (Fig. 1d). Vickers microhardness traverses of the thinner plates show a flat profile relative to the 22-mm plate, which has the greatest hardness range (72 HV) and hardness minima at quarter-depth (see Fig. 1e–g).

Charpy V-notch

The CVN DBTT_{KV} (KV represents the absorbed energy for instrumented CVN testing), LE (DBTT_{LE}), and the CVN FATT₅₀ and the upper shelf energy (USE) are presented in Fig. 2, along with fracture surfaces. Overall, the trends exhibited for each parameter for all three plates and specimen

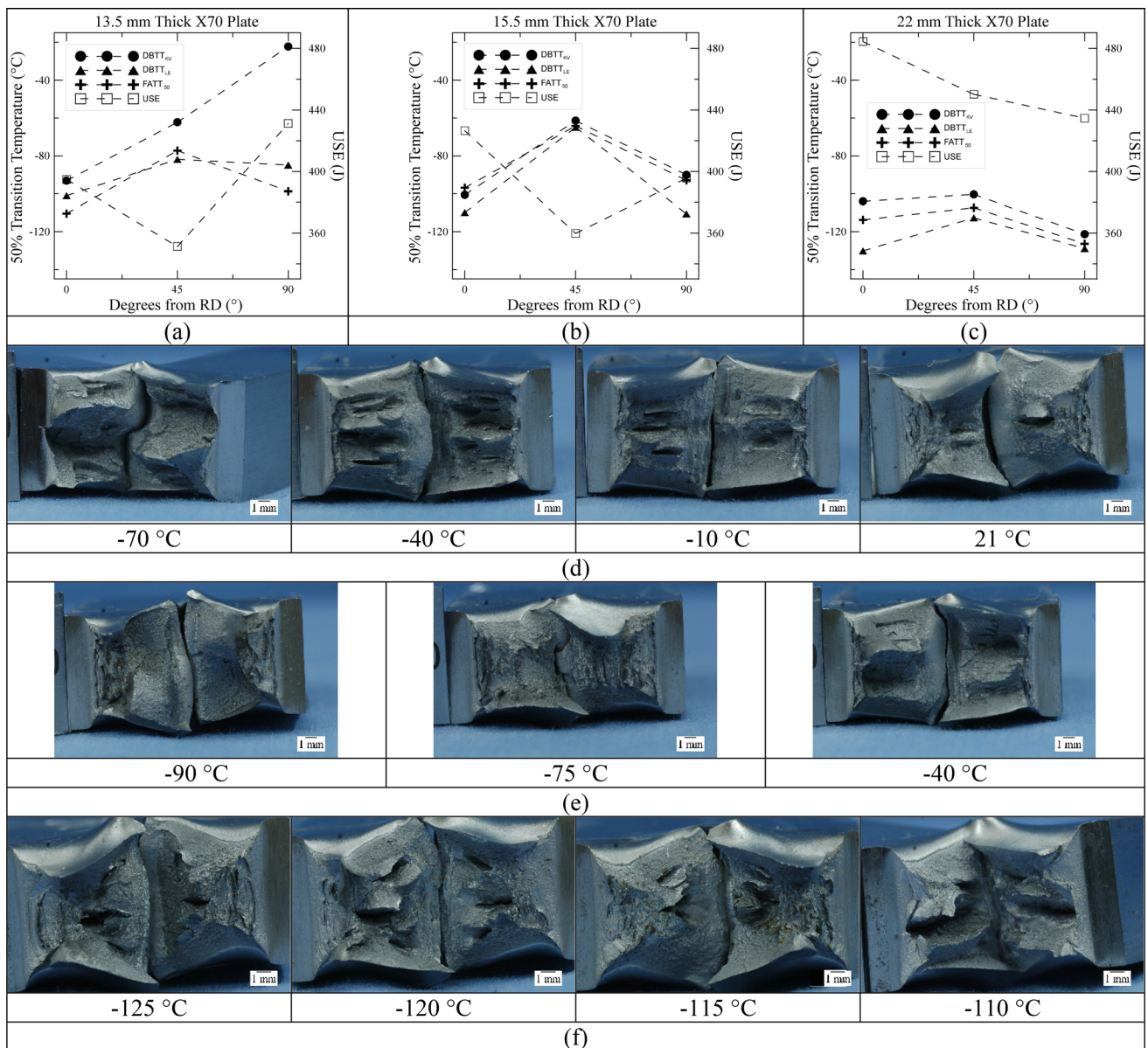


Fig. 2. CVN DBTT_{KV}, DBTT_{LE}, FATT₅₀, and USE versus orientation for the (a) 13.5-mm, (b) 15.5-mm, and (c) 22-mm plates, and CVN fracture surfaces of 90° orientation specimens tested at TTs for the (d) 13.5-mm, (e) 15.5-mm, and (f) 22-mm plates.

orientations are similar, although the DBTTs vary. The 22-mm plate has the lowest $DBTT_{KV}$, $DBTT_{LE}$, and $FATT_{50}$ and the highest USEs for all three plates and orientations. The 13.5-mm and 15.5-mm plates have similar, reduced toughness performance relative to the 22-mm plate. For most of the permutations of plate thickness, DBTTs, and USE, the 45° orientation exhibits reduced toughness performance (i.e., high DBTTs and low USEs). However, the 13.5-mm plate 90° orientation has the highest $DBTT_{KV}$ and the 22-mm plate 90° orientation has the lowest USE.

Only the 90° orientation CVN specimens exhibit separations for all plate thicknesses. The 90° orientation of the 13.5-mm and 22-mm plate CVN specimens tested at TTs exhibited the most separations (Fig. 2d and f), while the 15.5-mm plate 90° orientation CVN specimens tested at TTs only exhibit separations at -40°C (Fig. 2e). The 13.5-mm plate has the most CVN fracture surfaces that exhibit separations for all three orientations, while the 15.5-mm plate has the fewest CVN fracture surfaces with separations for all three orientations. The 22-mm plate 0° and 45° orientations have no separations, while the 90° orientation has multiple specimens exhibiting separations.

Drop-weight Tear Testing

The DWTT $DBTT_{85}$ for all three plates is shown in Fig. 3. For all three orientations, the 13.5-mm plate generally has the lowest $DBTT_{85}$, while the 15.5-mm plate has the highest. $DBTT_{85}$ varies with specimen orientation, with the thinner plates' 45° orientation specimens having higher $DBTT_{85}$, although the 22-mm plate does not exhibit significant orientation variations in $DBTT_{85}$. For all three plates and specimen orientations, the largest variation in SA measurements generally occurs at TTs, while upper and lower shelf region test temperatures (UST and LST, respectively) generally have less variation in SA. There is also an increase in separations on DWTT specimens tested at TTs which could contribute to the variation in SA ratings at TTs, because the presence of separations on fracture surfaces can further complicate the visual assessments performed to measure SA. Figure 3 shows DWTT UST and TT fracture surfaces that illustrate how separations affect the appearance of fracture surfaces. For all three plates and specimen orientations, SIs are higher at the centerline at USTs and TTs, as shown in Fig. 4. As the test temperature decreases into LST regimes, SIs at the quarter-depth begin to overtake centerline SIs, especially for the 90° orientation, which generally has higher SIs than the 0° or 45° orientations for all three plates at these test temperatures. At LSTs, SIs generally drop to zero because the fracture surfaces are dominated by cleavage fracture concentrated at the centerline, and separations did not form in the cleavage fracture areas. Samples with

areas of cleavage fracture only had separations in the non-cleavage areas. The 13.5-mm 90° orientation -70°C specimen exhibits this phenomenon, with separations present at the edge and quarter-depth, but not at the centerline (Fig. 4g). The 45° orientation generally has the lowest total SI for all three plates (see Fig. 5) but this is also temperature-dependent, as this trend is less pronounced at USTs and there is very little variation between specimens at LSTs, where the presence of separations generally decreases. The largest variation in SI measurements for all three plates occurs in the TT ranges.

Figures 4 and 5 show that the 13.5-mm plate generally has the highest SI. However, SI is not a good metric for comparing separation severity between plate thicknesses, because it is normalized by the inspected area. Therefore, thicker plates will have significantly lower SIs for the same measured separation length. Based on qualitative visual assessments, the 13.5-mm plate has the most separations throughout the through-thickness of the plate at a wide range of temperatures (Fig. 3a). The 22-mm plate appears to have fewer separations concentrated closer to the centerline at most USTs and TTs. However, the separations present in the 22-mm plate appear deeper and wider than those in the 13.5-mm plate (Fig. 3c).

DISCUSSION

Comparison of DWTT and CVN Results

DWTT was developed in the 1960s as a mill test to determine the $DBTT_{85}$ of ferritic steels, and it was found to produce fracture surfaces that closely matched full-scale pipe burst tests at the same temperatures.²¹ The SA of the DWTT specimen could then be used to estimate the full-scale fracture propagation mode. A series of full-scale pipe burst tests performed in the 1970s^{21,22} also determined that DWTT fracture resistance is related to the CVN absorbed energy that has the same SA and SFA as the full-scale fractured pipe, and that DWTT SAs can therefore be used to determine the CVN energy required for full-sized plates, as shown in Fig. 6. Note that SA and SFA are the same measurement of a fracture surface's shear area appearance, but are referred to as SA and SFA in standards for DWTT and CVN testing, respectively. The $DBTT$ for CVN testing is lower than for the DWTT at the same SA because of the difference in constraint.²¹

In this work, however, comparing DBTTs based on CVN and DWTT specimens shows that the two impact tests estimate different toughness performances for the same plates. The 22-mm plate has the lowest DBTTs and the highest USEs based on CVN testing (Fig. 2c), while the 13.5-mm plate generally has higher DBTTs and lower USEs (Fig. 2a). However, DWTT results for the 13.5-mm plate show that the thinner plate has some of the lowest $DBTT_{85}$ for all three plates (Fig. 3a). The

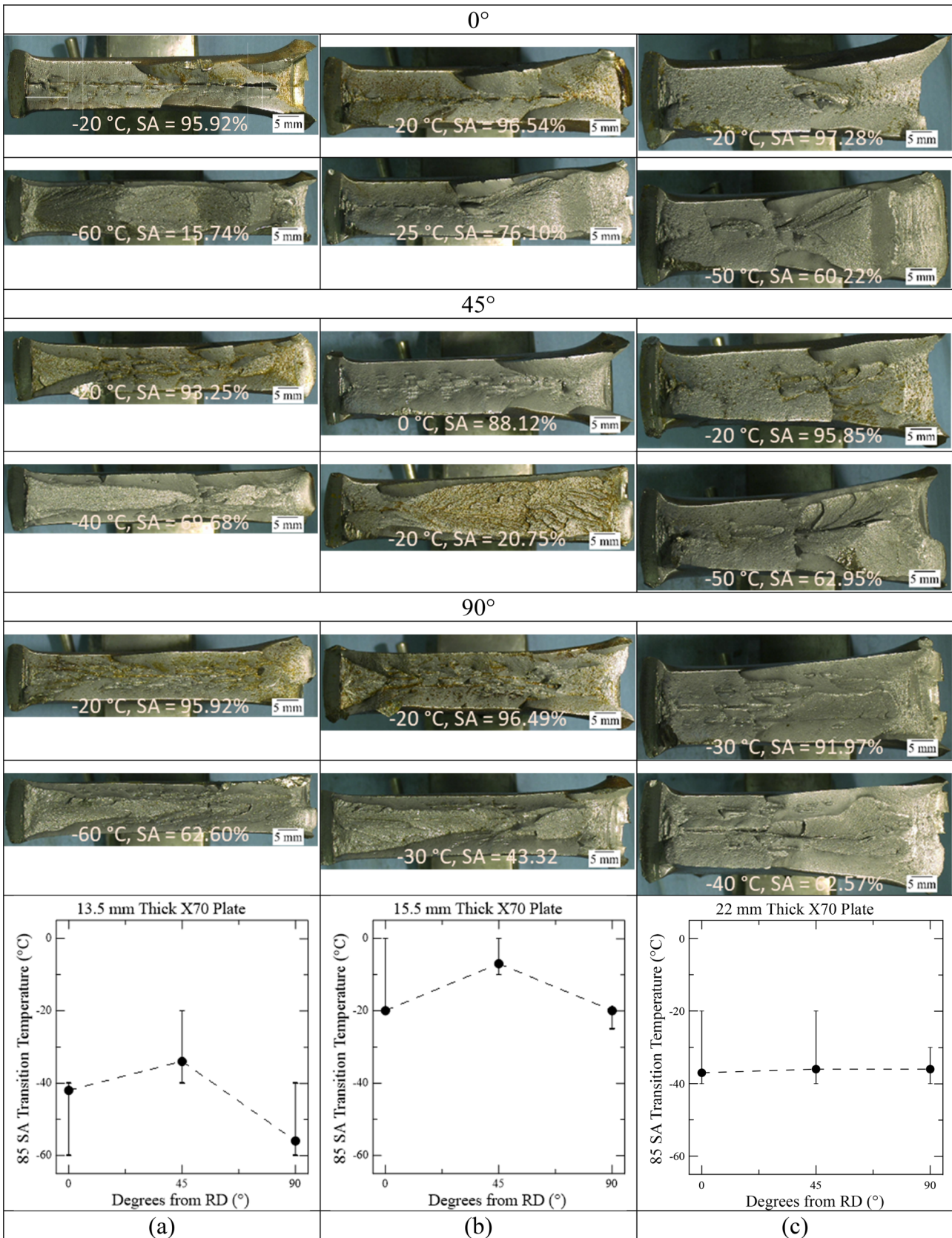


Fig. 3. DWTT fracture surfaces of the (a) 13.5-mm, (b) 15.5-mm, and (c) 22-mm plates exhibiting upper shelf SAs and transition region SAs and graphs of the DBTT₈₅ with respect to orientation. Images are organized in rows by orientation, starting with 0° and descending to 90°. Error bars the two contiguous temperatures between which the SA drops below 85%.

Microstructure and Thickness Effects on Impact Behavior and Separation Formation in X70 Pipeline Steel

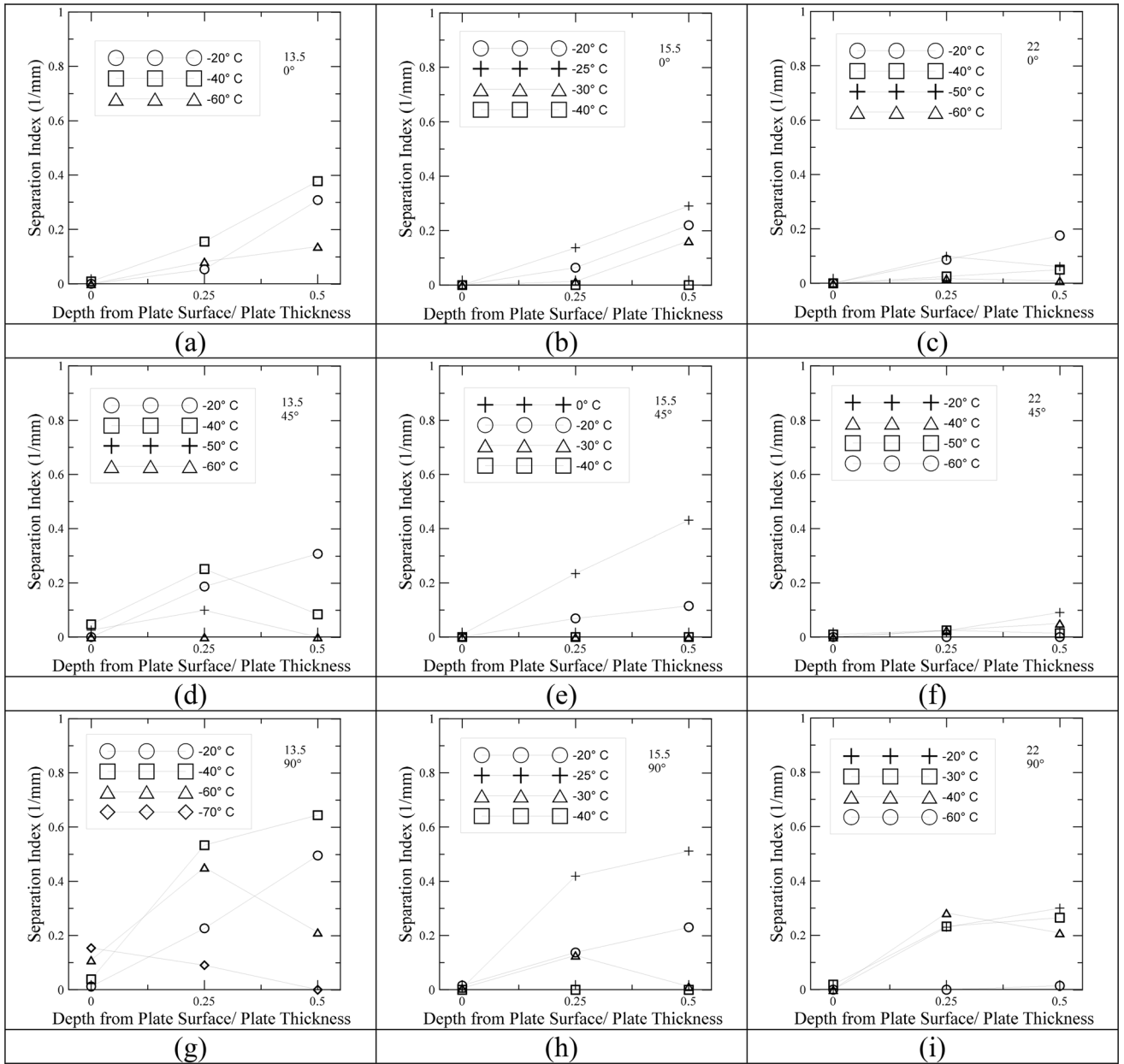


Fig. 4. DWTT SI versus depth from plate surface showing test temperature effects for the 13.5-mm plate in the (a) 0°, (d) 45°, (g) 90° orientations, the 15.5-mm plate in the (b) 0°, (e) 45°, (h) 90° orientations, and the 22-mm plate in the (c) 0°, (f) 45°, (i) 90° orientations.

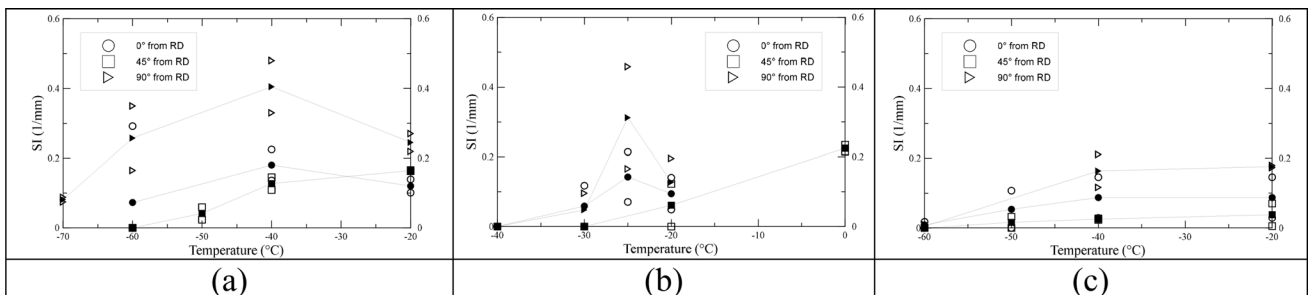


Fig. 5. SI versus test temperature for each specimen orientation: (a) 13.5-mm, (b) 15.5-mm, (c) and 22-mm plates; filled symbols represent data series averages.

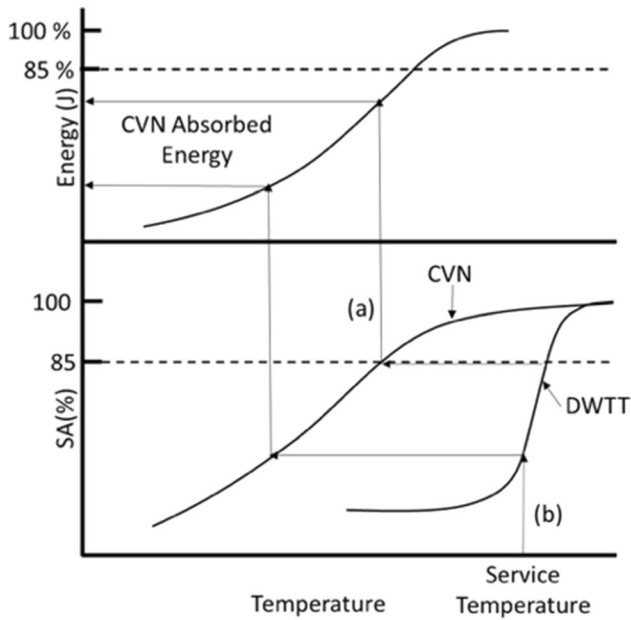


Fig. 6.. Relationship between CVN absorbed energy, CVN SFA, and DWTT SA at (a) 85% SA or (b) a set service temperature. Recreated from Ref. 22

following discussion compares CVN DBTTs estimated from the SFA and absorbed energy curves and then relates these two curves to the DWTT $DBTT_{85}$ curve using the method outlined in Fig. 6, with detailed data in Table III.

First, a comparison of the CVN SFA and absorbed energy curves was made by estimating the DBTT for each curve using 85% SFA and absorbed energy criteria to enable comparisons with DWTT SAs (Fig. 6a). $DBTT_{85}$ is a conservative value used for DWTT and focuses on when the fracture propagation mode transitions from mostly ductile to ductile/brittle SA appearance, whereas a 50% SFA DBTT is generally used for CVN testing DBTT estimates.^{23,24} To make a direct comparison, the $DBTT_{85}$ for the CVN SFA and absorbed energy curves were determined (Table III, columns 3 and 4). The energy curve indicates lower DBTTs for CVN versus DWTT for all three plates and orientations. The most significant example is 13.5 mm/45°, where the energy curve estimates a DBTT that is 77°C lower. Therefore, the CVN absorbed energy that matches an 85% CVN SFA and used to calculate fracture resistance would correlate with a DWTT test temperature that would be significantly above the 85% upper shelf region limit of most of these plates. This could lead to an artificially high estimate of fracture resistance, since advanced higher-toughness steels require large initiation energies that can increase CVN absorbed energy results.²¹ There is no simple physical correlation explaining why the CVN SFA and CVN energy DBTT curves should correspond to each other,²⁴ and these results highlight the potential difference between these two estimates. Absorbed

energy is easier to measure, but gives no indication of fracture appearance, while SA is more difficult to measure, but indicates the fracture mode at a given temperature.²⁴ Another method for evaluating CVN DBTT is LE, and comparison of the absorbed energy and LE results also indicate differences between DBTTs estimated using these two methods, the most notable being the difference between $DBTT_{KV}$ and $DBTT_{LE}$ for the 13.5-mm and 22-mm plates 90° and 0° orientations, respectively (Fig. 2a and c).

Second, the CVN results show that the lower toughness material conditions (i.e., the 15.5-mm plate and 45° orientation) follow the empirical correlations between CVN SFA and the absorbed energy better than the higher-toughness material conditions. The CVN absorbed energy at the $DBTT_{85}$ from SA is listed in Table III, column 5, and shown as the % of USE (Table III, column 6) as a way to further highlight the differences between the CVN SFA and energy curves; ideally, the % absorbed energy/USE would be $\geq 85\%$ (i.e., both curves estimate upper shelf behavior). The 15.5-mm plate and all 45° orientation CVNs exhibit CVN energies $\geq 85\%$ of the USE, but all other orientations for the 13.5-mm and 22-mm plates have CVN absorbed energies at 85% SA that are significantly lower than 85% of the USE. The 15.5-mm plate has the least complex microstructure (consisting mainly of PF), the highest DWTT $DBTT_{85}$, and has the most similar DWTT toughness performance to the ferritic steels that were used to develop the correlations between DWTT and CVN testing.²¹ This is likely why the estimated CVN absorbed energy and USE values for this steel are in good agreement. The 45° orientation generally has a higher DBTT than other orientations. The lower relative toughness in this orientation could explain why the 45° orientation estimated CVN absorbed energy and USE values are in agreement, since the relationship was developed for lower-toughness steels.

Finally, DWTT specifications for plates generally give a service temperature where 85% SA must be achieved. The data from these plates suggest that neither CVN SFA nor absorbed energy curves correlate well to DWTT results in plates with more complex microstructures. To show this, a similar analysis was performed considering a set service temperature of -30°C instead of a set SA of 85%. The results are displayed in the bottom half of Table III, columns 3–6. The -30°C service temperature is above the DWTT $DBTT_{85}$ for the 13.5-mm and 22-mm plates ($-56^{\circ}\text{C}/90^{\circ}$ and $-36^{\circ}\text{C}/90^{\circ}$, respectively), but falls below the DWTT $DBTT_{85}$ for the 15.5-mm plate ($-20^{\circ}\text{C}/90^{\circ}$) (see Fig. 3). The DWTT SA at -30°C is compared to the CVN absorbed energy curve by following the arrows labeled (b) in Fig. 6. The CVN absorbed energy determined following this technique can then be turned into a percentage of the CVN USE (bottom half of Table III, column 6), providing a comparison of the DWTT and CVN behavior at a representative

Table III. CVN absorbed energy correlated with DWTT SA

1 Plate (mm)	2 Orientation	3 DBTT ₈₅ based on CVN SFA (°C)	4 DBTT ₈₅ based on CVN absorbed energy (°C)	5 CVN absorbed energy at CVN SFA DBTT ₈₅ (J)	6 CVN absorbed energy/USE (%)
13.5	0°	-110	-116	108	27
	45°	-7	-84	334	95
	90°	-27	-79	204	47
15.5	0°	-54	-115	423	99
	45°	-38	-64	360	100
	90°	-57	-96	395	100
22	0°	-80	-136	365	75
	45°	-94	-101	450	100
	90°	-123	-131	186.18	43

Plate (mm)	Orientation	DWTT SA at -30 °C (%)	CVN temperature with equivalent SFA as DWTT (°C)	CVN absorbed energy at CVN temperature (i.e., column 4) (J)	CVN absorbed energy/USE (%)
13.5	0°	95.40	-110	108	27
	45°	90.12	-3	337	96
	90°	95.58	19	319	74
15.5	0°	44.61	-102	199	47
	45°	18.42	-83	7	2
	90°	57.58	-84	323	82
22	0°	93.87	-62	426	88
	45°	91.34	-89	450	100
	90°	90.30	-123	199	46

service temperature. By comparing where the CVN absorbed energy falls on the CVN absorbed energy curve to the region where the DWTT SA falls on the DWTT SA curve, it can be qualitatively determined if the CVN and DWTT curves would estimate similar DBTT behavior (i.e., compare columns 3 and 6 in the bottom half of Table III). With the exception of the 15.5-mm plate and all of the 45° orientation results, the CVN absorbed energy curves generally exhibit lower shelf region and transition behavior (CVN absorbed energy/USE < 85%) at the CVN temperature that correlates to the service temperature, while the DWTT SA curves exhibit upper shelf behavior (SA > 85%) at the service temperature. Again, the ferritic 15.5-mm plate results follow the empirical correlations better than the 13.5-mm and 22-mm plates, with the PF + pearlite or bainitic microstructures, respectively. The lowest toughness orientation (i.e., 45°) results also follow the empirical correlations better than the higher-toughness orientations.

These results show that the test/analysis methods selected to analyze the toughness of a plate change apparent performance. In addition to there being no simple physical way to correlate CVN SFA and absorbed energy curves, there is no simple physical reason for the DWTT curve to align with either of the CVN curves. Thus, for the more complex microstructures and higher toughness steels (i.e.,

the 13.5-mm and 22-mm plates), the previously developed empirical relationships between CVN SFA, CVN absorbed energy, and DWTT SA did not accurately estimate their toughness behavior. Even when a set service temperature is examined, rather than a set SA, the difference in the curves significantly affects the estimated impact behavior, except for the lowest toughness conditions (i.e., the 15.5-mm plate and 45° orientation) where the empirical relationships still show a qualitative relationship between CVN SFA, absorbed energy, and DWTT SA. The relationship between DWTT and CVN shown in Fig. 6 is empirical and based on numerous studies that involved DWTT, CVN testing, and full-scale pipe burst testing in the 1960s and 1970s.^{21,22} These relationships have not been examined for newer, higher-strength and -toughness materials. The results of the CVN testing and DWTT in this study suggest that, as both the toughness and the microstructural complexity of the steel increases, the previously established empirical relationships between the two tests no longer accurately correlate them and they cannot be used individually as a rigorous method of pipeline quality assurance.

In addition to increasing toughness and microstructural complexity, increasing plate thickness affects the mechanics of the DWTT and final SA analysis, whereas CVN geometry remains the

same. Therefore, a 22-mm plate DWTT specimen will have nearly double the fracture surface area of a 13.5-mm plate. CVN testing found that the 22-mm plate had better toughness than the 13.5-mm plate, but DWTT had opposite results: the 13.5-mm plate generally had the lowest DBTTs (Fig. 3). Since the 22-mm plate DWTT specimen has more material constraint than the 13.5-mm plate, a higher fracture initiation energy may be required to begin fracture propagation in the thicker plate, regardless of the actual material toughness, so DWTT of thicker plates may represent a lower-energy estimate of fracture propagation, since a larger proportion of the drop weight energy is consumed by fracture initiation.

The purpose of DWTT is to evaluate the propagation resistance of pipeline steels. Correlations for fracture initiation or propagation energy of a steel must consider the contributions of all components that make up impact energy (e.g., initiation, propagation, and kinetic/throw energy).²¹ High fracture initiation energy has been found to skew the interpretation of the impact energy contributions in both CVN and DWTT by artificially increasing the estimated propagation resistance, as well as estimating a false DBTT.²¹ The high fracture initiation energy required to start a crack in advanced and thicker pipeline steels can also affect the mechanics of the DWTT, and has been linked to a fracture appearance phenomenon called inverse fracture (IF), which is defined in this study as the reappearance of cleavage at the end of fractures due to work-hardening.^{23,25-27} The high toughness of advanced pipeline steels resists the traditional brittle fracture initiation seen in DWTT of lower-toughness steels and delays fracture initiation.²⁶ This delay has been observed using high-speed cameras of DWTT that show the specimen bending significantly before the crack initiates.²⁶ The footage also shows that this initiation is often followed by crack arrest and additional significant bending of the remaining ligament until the specimen finally fails. Bending of the DWTT specimen results in work-hardening of the steel ahead of the crack, especially in the remaining ligament after crack arrest. Hardness testing on broken DWTT specimens has shown that this remaining ligament is where the majority of work-hardening occurs.^{23,26,28} Hwang et al.²³ determined that the area of the fracture surface that exhibits IF can be directly correlated to the presence of work-hardening in a DWTT specimen. The presence of IF reduces the accuracy of SA measurements made on thicker plate DWTT fracture surfaces that require higher fracture initiation energies, and was observed in nearly 50% of the 22-mm plate DWTT fracture surfaces, while the 13.5-mm and 15.5-mm plates only exhibited IF in ~20% of specimens. The increased presence of IF in the 22-mm plate potentially explains the difference between toughness performance estimated by CVN and DWTT, and suggests

that the DWTT SA DBTT estimate may be more representative of a work-hardened 22-mm plate.

Toughness Anisotropy

The 22-mm plate generally exhibits the least amount of toughness anisotropy among specimen orientations, especially in the DWTT results, and has the most banded microstructure with hardness variation in the through-thickness direction. Banded microstructures, including bainitic bands, and crystallographic texture anisotropy have often been cited as promoting separation formation and correlating to toughness anisotropy.^{3,7-9,13,14} Banding generally occurs because of chemical segregation, with detectable variations in manganese content in the plate through-thickness. Energy-dispersive X-ray spectroscopy investigation of the 22-mm plate suggests that there is no significant increase in manganese content in the bainitic bands or across the plate through-thickness. Therefore, the type of microstructural banding in this plate may not be severe enough to promote separation formation that could cause toughness anisotropy. It is interesting to note that the 13.5-mm and 15.5-mm plates both exhibit toughness anisotropy with increased DBTTs in the 45° orientation, even though they have relatively homogeneous microstructures and hardness profiles, suggesting that crystallographic texture could have a significant role in controlling toughness anisotropy. A study conducted by Joo et al.,¹⁰ designed to isolate the role of crystallographic texture on toughness anisotropy in X80 steels, found that when banding, and subsequently separations, were eliminated through heat treatment, there was still significant variation in impact toughness between CVN specimen orientations. Crystallographic texture was identified as the primary cause of toughness anisotropy in the study.¹⁰

Separations

The presence of separations makes performing accurate SFA and SA measurements difficult, and there is no simple or standard way to measure how much energy is redirected from the crack tip when they form.²⁰ This makes it more difficult to assess the SFA, SA, and absorbed energy of both CVN and DWTT specimens. The 13.5-mm plate generally exhibited the most separations in CVN specimens for every orientation tested. The factors that have been suggested to contribute to separations are microstructural banding, inclusions/stringers, constraint, and crystallographic texture.^{3,7-9,13,14} The 13.5-mm plate did not exhibit significant microstructural banding, had a similar inclusion content to the other plates, and had the lowest constraint, suggesting that crystallographic texture may be a primary factor controlling separation formation in this material. The 15.5-mm plate had very few CVN specimens with separations. It also

has a less complex ferritic microstructure without obvious banding, similar to the ferritic steels used in the 1970s to develop impact testing that did not develop separations.²¹ The 22-mm plate only exhibited separations on 90° orientation CVN specimens, even though the microstructure was banded and there was significant variation in hardness in the through-thickness.

The 90° orientation was the only CVN specimen orientation that exhibited separations for all three plates, and there is also an increase in the total SI for all the DWTT specimens tested in the 90° orientation (Fig. 5). The 0° orientation also exhibited separations, especially in the 13.5-mm plate. Similar crystallographic texture components that promote separation formation that are formed by rolling could be observed in both the 90° and 0° specimen orientations because of the symmetry imposed by an orthorhombic–cubic sample-crystal structure system. This offers a potential explanation for the higher number of separations and SIs observed in both these specimen orientations when compared to the 45° orientation. The increased presence of separations in the 90° orientation for both impact tests suggests that textures that develop during rolling are aligned in the plane of separation formation in 90° orientation specimens, thus promoting separations. High intensities of texture components in the {001} plane family have been found to promote separation formation because they orient cleavage planes parallel to a plate's rolling plane (i.e., the plane of separation formation).^{5,13,29}

Through-thickness SI results for all three plates (Fig. 4) confirm the effect of out-of-plane constraint (T_z) on the location of separation formation. High SIs at the centerline of the plates tested at USTs and TTs indicate that separations may be releasing the high T_z present at the centerline of the plates. The increase in quarter-depth separations seen in specimens tested at lower TTs can be explained by the presence of fewer, but deeper (i.e., more severe), centerline separations that would be measured as a lower SI, or the presence of cleavage fractures along the centerline. Both would reduce T_z along the centerline and move the T_z maximum to the quarter-depth, causing separations to develop at the quarter-depth to relieve this increased T_z .¹⁴ Since the effect of constraint is apparent in all three plates, regardless of microstructure and hardness variation in the through-thickness, it is possible that T_z is a primary factor determining the location of separation formation. Separations form primarily along the centerline of the plate, and only appear at the quarter-depth location after a centerline separation has formed or if the centerline is dominated by cleavage.

There is no generally agreed-upon method for measuring separation severity, and most proposed methods for quantifying them face limitations. The SI measurement method²⁰ does not scale

appropriately with increasing plate thickness, because it is a measurement that is normalized by an inspected area that increases with plate thickness and therefore cannot compare separation severity between plate thicknesses. The SI measurement method also cannot properly account for the severity/morphology of separations that have significant width or depth. Visual inspection and cross-sectioning of some of the 22-mm plate DWTT fracture surfaces revealed deep centerline separations that would require significant energy to form, but this has not been quantified using the SI method. 3D surface profiling methods such as white light interferometry can be used to measure fracture surface topography, but CVN and especially DWTT fracture surfaces of advanced pipeline steels are topographically complex, sometimes with overlapping features and very thin separations that cannot be properly interrogated using white light interferometry. 3D surface profiling techniques also have additional equipment and time requirements that are not conducive to mill environments. Presently, the most effective way to determine separation severity is still a qualitative visual assessment.

CONCLUSION

The following findings may be drawn from this study:

- (i) Microstructural banding does not promote separation formation in the three steel plates investigated.
- (ii) Separation formation is enhanced in the 90° orientation, likely due to textures that develop during rolling, which align with the plane of separation formation in this specimen orientation.
- (iii) The SI measurement method suggests that T_z may have an effect on the location of separation formation during DWTT. Separations likely form at the centerline to release the maximized T_z present, regardless of microstructure and hardness variation in the plate through-thickness, suggesting that constraint may have a greater role than microstructure in the location of separation formation.
- (iv) The SI measurement method does not scale with increasing plate thickness and artificially increases the SI of thinner plates, so SIs should not be compared between plates of different thicknesses.
- (v) SFA, absorbed energy, and LE from CVN tests do not estimate the same DBTT behavior. In this study, CVN absorbed energy DBTT estimates are not conservative with respect to the DBTT obtained from SA measurements.
- (vi) As the toughness and microstructural complexity of steels increases, the empirical

relationships originally developed to relate CVN, DWTT, and full-scale pipe burst testing no longer seem to apply. Agreement between the estimated toughness behavior only occurred for the lowest toughness conditions (i.e., the 15.5-mm plate and 45° orientation). Therefore, CVN and DWTT testing cannot be used individually as a rigorous method of pipeline quality assurance, and new empirical relationships need to be developed for high-toughness steels.

ACKNOWLEDGEMENTS

The author would like to acknowledge SABIC for providing the 13.5-mm and 15.5-mm plates and Baosteel for providing the 22-mm plate. The author would also like to thank EVRAZ North America for performing all DWT testing, and the National Institute of Standards and Technology (NIST) for performing all CVN testing. Finally, the author would like to thank colleagues and sponsors of the Advanced Steel Processing and Products Research Center at the Colorado School of Mines for their support. Commercial equipment, instrument, or materials are identified only in order to adequately specify certain procedures. In no case does such identification imply recommendation or endorsement by NIST. On behalf of all authors, the corresponding author states that there is no conflict of interest.

CONFLICT OF INTEREST

The authors declare that they have no conflicts of interest.

REFERENCES

- H. Hillenbrand, M. Graf, and C. Kalwa, *Proceedings of the Niobium Science and Technology Conference*, 543 (2001).
- J. Ding, X. Liang, and S. Jiao, 9, 35 (Baosteel Technical Research, Shanghai, China, 2015).
- S.Y. Shin, B. Hwang, S. Kim, and S. Lee, S.Y. Shin, B. Hwang, S. Kim, and S. Lee, *Mater. Sci. Eng. A* 429, 196. (2006).
- D.B. Rosado, W. De Waele, and D. Vanderschueren, D.B. Rosado, W. De Waele, and D. Vanderschueren, *Int. J. Sustain. Construct. Design* 4, 1. (2013).
- H. M. Al-Jabr, Colorado School of Mines Metallurgical and Materials Engineering, Golden, CO, PhD Thesis 2016.
- B. Hwang, Y. Gon Kim, S. Lee, Y. Min Kim, N.J. Kim, and J. Yong Yoo, B. Hwang, Y. Gon Kim, S. Lee, Y. Min Kim, N.J. Kim, and J. Yong Yoo, *Metall. Mater. Trans. A* 36A, 2107. (2005).
- A.P. Coldren, and J.L. Mihelich, A.P. Coldren, and J.L. Mihelich, *Metaltoved. Termichesk. ObrabotkaMetatlov* 7, 44. (1977).
- S. Li, Z. Jiang, Y. Li, D. Stalheim, Q. Li, and G. Zhang, in *Proceedings of the 9th International Pipeline Conference*, vol. 293 (2012).
- X.L. Yang, Y.-B. Xu, X.-D. Tan, and D. Wu, X.L. Yang, Y.-B. Xu, X.-D. Tan, and D. Wu, *Mater. Sci. Eng. A* 607, 53. (2014).
- M.S. Joo, D.W. Suh, J.H. Bae, N. Sanchez Mouriño, R. Petrov, L.A.I. Kestens, and H.K.D.H. Bhadeshia, M.S. Joo, D.W. Suh, J.H. Bae, N. Sanchez Mouriño, R. Petrov, L.A.I. Kestens, and H.K.D.H. Bhadeshia, *Mater. Sci. Eng. A* 556, 601. (2012).
- M.S. Joo, D.-W. Suh, J.H. Bae, and H.K.D.H. Bhadeshia, M.S. Joo, D.-W. Suh, J.H. Bae, and H.K.D.H. Bhadeshia, *Mater. Sci. Eng. A* 546, 314. (2012).
- S.Y. Shin, B. Hwang, S. Lee, N.J. Kim, and S.S. Ahn, S.Y. Shin, B. Hwang, S. Lee, N.J. Kim, and S.S. Ahn, *Mater. Sci. Eng. A* 458, 281. (2007).
- A. Gervasyev, I. Pyshmintsev, A. Struin, T. Yesiev, and A. Arabey, in *Pipeline Technology Conference*, vol. 1 (2013).
- W. Guo, H. Dong, M. Lu, and X. Zhao, W. Guo, H. Dong, M. Lu, and X. Zhao, *Int. J. Press. Vessel. Pip.* 79, 403. (2002).
- ASTM E562, ASTM International, West Conshohocken, PA, (2011).
- ASTM E112, ASTM International, West Conshohocken, PA, (2013).
- ASTM E23, ASTM International, West Conshohocken, PA, (2018).
- API RP 5L3, API, Washington, DC, (1996).
- ASTM E436, ASTM International, West Conshohocken, PA, (2014).
- B. Davis, University of Wollongong School of Mechanical, Materials, Mechatronic, and Biomedical Engineering, Ph.D. Thesis, (2017).
- G. Wilkowski, W. Maxey, and R. Eiber, *A.G.A.-EPRG Line Pipe Research Seminar III*, 1 (1978).
- M. Erdelen-Peppler, R. Gehrman, G. Junker, G. Knauf, and A. Liessem, in *11th International Conference on Fracture* (2005).
- B. Hwang, S. Lee, Y.M. Kim, N.J. Kim, J.Y. Yoo, and C.S. Woo, B. Hwang, S. Lee, Y.M. Kim, N.J. Kim, J.Y. Yoo, and C.S. Woo, *Mater. Sci. Eng. A* 368, 18. (2004).
- M. Manahan, and C. McCowan, M. Manahan, and C. McCowan, *J. ASTM Int.* 5, 1. (2008).
- Y. Hioe, G. Wilkowski, M. Fishman, and M. Myers, in *Proceedings of the 11th International Pipeline Conference*, V003T05A015 (2016).
- M. Connelly, J. Hammond, and S. Schmidt, White Paper, API SC5/Task Group on Line Pipe and the European Pipeline Research Group, vol. 1 (2011).
- B. Hwang, S. Lee, Y. M. Kim, and N. J. Kim, in *Proceedings of The Thirteenth International Offshore and Polar Engineering Conference*, vol. 129 (2003).
- E. B. Mitchell, Colorado School of Mines Metallurgical and Materials Engineering, Golden, CO, MS Thesis, (2019).
- G.J. Baczynski, J.J. Jonas, and L.E. Collins, G.J. Baczynski, J.J. Jonas, and L.E. Collins, *Metall. Mater. Trans. A* 30A, 3045. (1999).

Publisher's Note Springer Nature remains neutral with regard to jurisdictional claims in published maps and institutional affiliations.